# Ultrafine eutectic Ti-Fe-based alloys processed by additive manufacturing – A new candidate for high temperature applications

## Supplementary material

Joachim Gussone[1,*], Katrin. Bugelnig[1], Pere Barriobero-Vila[1], Julio Cesar da Silva[2,6], Ulrike Hecht[3], Christian Dresbach[4], Federico Sket[5], Peter Cloetens[6], Andreas Stark[7], Norbert. Schell[7], Jan Haubrich[1], Guillermo Requena[1,8]

[1] German Aerospace Center DLR, Institute of Materials Research, Linder Höhe, 51147 Cologne, Germany

[2] Institut Néel CNRS UPR2940, 25 Avenue des Martyrs BP 166, 38042 Grenoble, France

[3] Access e.V., Intzestr. 5, 52072 Aachen, Germany

[4] University of Applied Sciences Bonn-Rhein-Sieg, Von-Liebig Str. 20, 53359 Rheinbach, Germany

[5] IMDEA Materiales, Eric Kandel 2, Tecnogetafe, 28906 Getafe, Madrid, Spain

[6] European Synchrotron Radiation Facility, 71, Avenue des Martyrs, 38043 Grenoble, France

[7] Helmholtz-Zentrum Geesthacht, Max-Planck-Straße 1, 21502 Geesthacht, Germany

[8] RWTH Aachen University, Metallic Structures and Materials Systems for Aerospace Engineering, D-52062 Aachen, Germany

### A1. NF-PXCT experiments

During the experiments, the samples were under vacuum (~ $10^{-7}$ mbar) at room temperature. A FReLoN indirect detector system [1] with 4096 × 4096 pixels and a GGG:Eu scintillator were used to record the images. The physical pixel size of the CCD was 15 μm, which was magnified by a factor 10 using a visible light optics between the scintillator and the CCD. The recorded images were further binned by a factor 2, which results in a pixel size of 3 μm on the detector and an array of 2048 × 2048 pixels. The detector was placed at $z_{12} = z_1 + z_2 = 1.208$ m downstream the X-ray focus position, where $z_1$ is the focus-to-sample distance and $z_2$ is the sample-to-detector

distance. The sample was placed at $z_1$ = 6.04 mm downstream the focus, and the beam divergence after the focus was 5.5 mrad. The images acquired in this configuration are inline holograms with a pixel size of 15 nm yielded by the magnification factor of $z_{12}/z_1$ = 200× due to the divergent beam. The X-ray photon energy was set to 17.05 keV with 1% bandwidth.

The surface features of the multilayer coated Kirkpatrick-Baez (KB) optics create a structured X-ray beam at the sample position. Near-field ptychography exploits this structured illumination for efficient phase retrieval from the inline holograms [2]. The tomographic scan was performed over 180 degrees using a binary acquisition scheme as described by Kaestner et al. [3] with 4 nests of projections.

800 projections (4 nests of 200 projections) were acquired for the sample extracted from the region with fine structures in the sub-micrometre range which mainly consist of β-Ti and TiFe, while 1000 projections (4 nests of 250 projections) were acquired for the sample extracted from the region containing η-$Ti_4Fe_2O_x$ dendrites. Each ptychographic scan is composed of 17 Fresnel diffraction patterns in the holographic regime recorded for different transverse shifts of the sample with respect to the incident illumination up to a maximum of 350 pixels. The scan grid is similar to the pseudo-random grid used by Stockmar et al. [2] with an additional scan point at the centre. The exposure time of each scan point was 0.2 s and, considering the movement of the motors and the detector readout time, the acquisition time of each projection was 30 s. At each scan, 5 images are also acquired without beam to take into account the dark noise of the CCD detector. The average image of those 5 dark images was subtracted from each of the 17 sample scan images.

## A2. NF-PXCT data processing

The ptychography phase retrieval of each projection was performed using the Python package Ptypy [4]. To accelerate the calculations, we binned the images by a factor 2 and 2,000 iterations of the difference map algorithm were used [5] to retrieve the phases. Thereafter, the resulting images were interpolated back to the original image size and used as initial guess to the difference map algorithm for 2,000 additional iterations. This was followed by 300 iterations of the maximum likelihood refinement [6]. The resulting projections with pixel size of 15 nm were then processed and aligned for the tomographic reconstruction according to methods previously described [7,8]. Afterwards, the tomographic reconstruction was performed on the phase projections using a modified filtered backprojection algorithm (FBP) with a Hilbert filter to circumvent phase unwrapping [7,8]. The final size of the reconstructed volumes was 2328 × 2357 × 2357 voxels, which correspond to volumes of 34.92 × 35.36 × 35.36 $\mu m^3$.

### Estimation of spatial resolution

The spatial resolution of the NF-PXCT reconstructed 3D images was determined using the Fourier Shell Correlation (FSC) method [9]. The results are displayed in Fig. S1. The spatial resolution is estimated from the division of the voxel size of 15 nm by the abscissa value of the intersection between the FSC curves with the 1/2-bit threshold curve indicated in each sub-figure. The estimated resolution was 39 nm (Fig. S1a) for the the eutectic-rich (ER) region and 48 nm (Fig. S1b) for the dendritic-rich (DR) region.

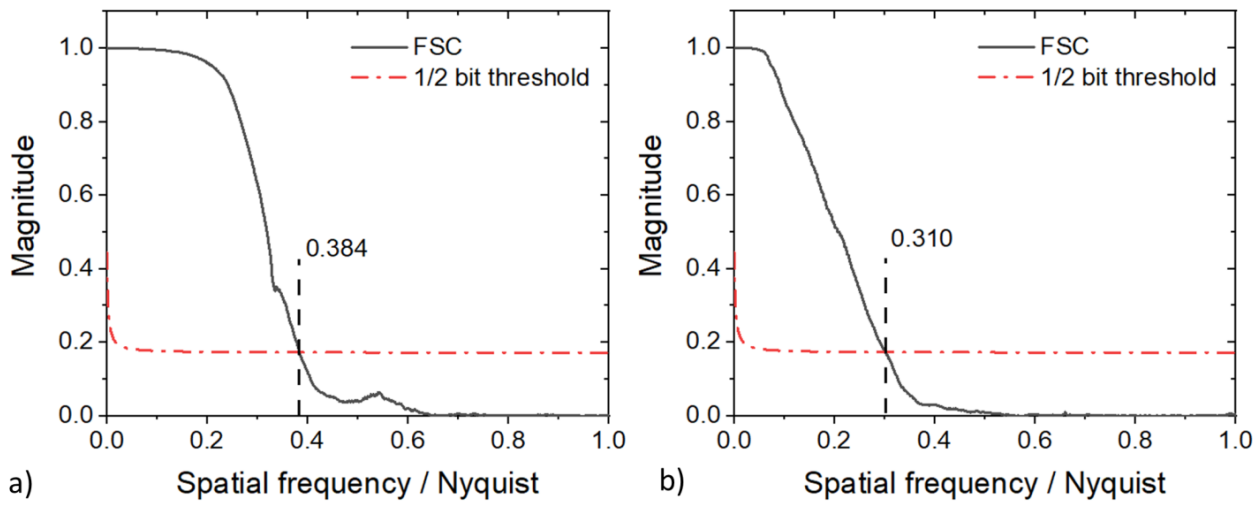


**Fig. S1: Estimation of the spatial resolution of the NF-PXCT images using the Fourier Shell Correlation method: Eutectic-rich (ER) region (a) dendritic-rich (DR) region (b). The intersection between the Fourier Shell correlation curves and the 1/2-bit threshold curve are indicated in each Figure.**

## A3. NF-PXCT segmentation workflow

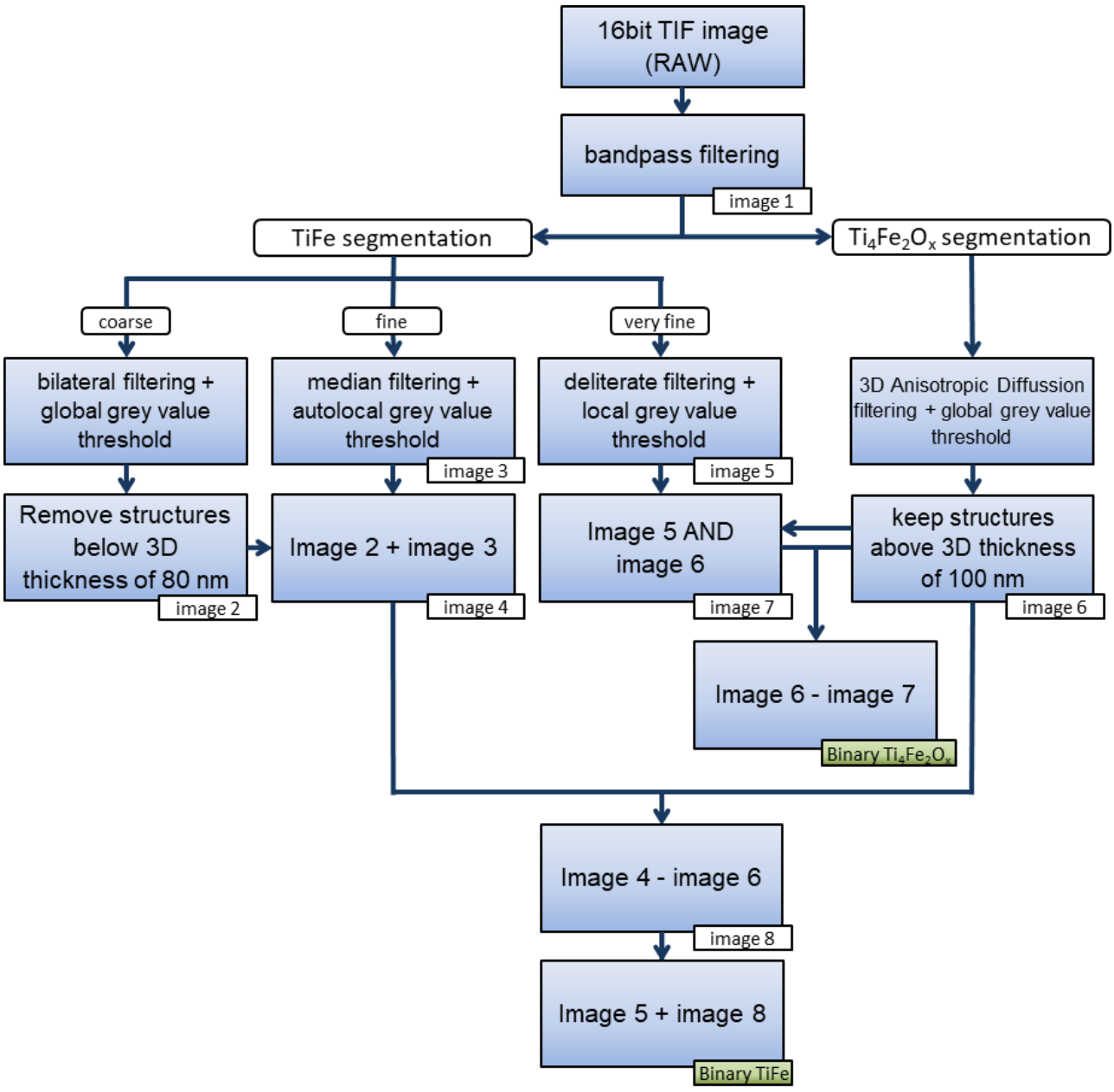


**Fig. S2: Workflow applied for the segmentation of the phases TiFe and η-$Ti_4Fe_2O_x$.**

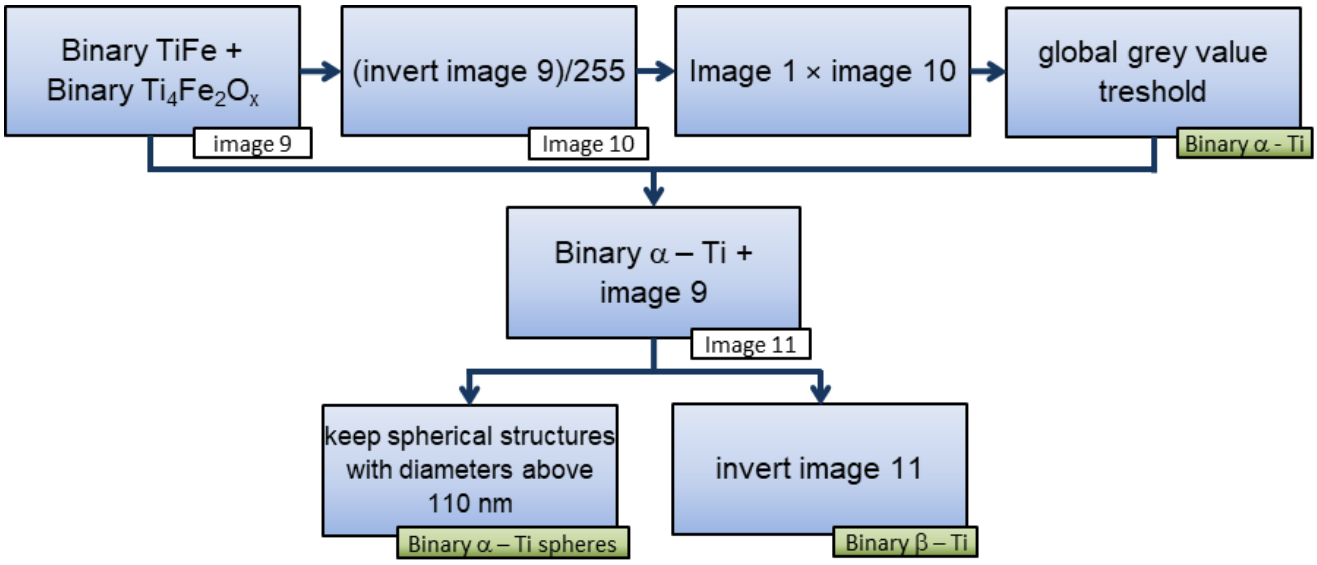


**Fig. S3: Workflow applied for the segmentation of the phases α-Ti and β-Ti.**

### A4. Calculation of density from NF-PXCT and 3D image analysis

First, the refractive index decrement δ, i.e. the correction to the real part of the complex refractive index n = 1 - δ + iβ, was determined voxel-wise from the images (Eq. 1):

$$\delta = (\delta_H - \delta_L) \cdot \left(\frac{\omega}{2^{16}-1}\right) + \delta_L \qquad \text{Eq. 1}$$

where ω is the grey value of the voxel, and $\delta_L$ and $\delta_H$ are the minimum and the maximum values of the refractive index decrement in the tomogram, respectively. Then, the actual mass density (ρ) of each voxel was calculated considering the segmentation masks of each phase (Eq. 2):

$$\rho = \left[\frac{2 \cdot 10^{-6} \cdot \pi \cdot \delta}{r_0 \cdot NA \cdot \lambda^2}\right] \cdot \left(\frac{A}{Z}\right) \qquad \text{Eq. 2}$$

where $r_0$ is the classical electron radius, NA is the Avogadro number, $\lambda$ = 0.7273 Å is the X-rays wavelength used during the ptychographic scans, and $\left(\frac{A}{Z}\right)$ is the ratio between atomic weight and

atomic number for the corresponding phase. The ratio $\left(\frac{A}{Z}\right)$ is 2.1773, 2.1614, 2.1773, and 2.1574 for the phases α-Ti, TiFe, β-Ti, and η-$Ti_4Fe_2O_x$, respectively. As these values are nearly identical, the grey values in the tomograms are essentially proportional to the mass density of the phase.

The 3D thickness distribution of each segmented phase was determined using Avizo Fire 9.5 as the diameter of the largest sphere that fits into the segmented phase at each voxel of its skeleton; details can be found in the work of Hildebrand and Rüegsegger [10].

**A5. HEXRD analysis**

Rietveld analysis using the software TOPAS 5 provided mass fractions and lattice parameters of the microstructural constituents. Mass densities of β-Ti (bcc, Im-3m) and TiFe (bcc, Pm-3m) were calculated by determining the lattice parameters in a first refining step. The iron content ($C_{Fe}$, at.%) was obtained assuming that the lattice parameters result from the composition of the phases (Ti and Fe contents) and that residual stresses are negligible for HT-LPBF at ~ 600 °C [11].

The refinement was subsequently carried out with the corresponding site occupancy for β-Ti and TiFe, while the values from Rupp and Fischer [12] were considered for the oxygen stabilized $Ti_2Fe$ phase (fcc, Fd3m). It should be pointed out that the existence of metastable $Ti_2Fe$ without oxygen stabilization has been a matter of debate [13-16]. Taking into account that the Ti/Fe ratio was close to 2 according to energy dispersive X-ray spectroscopy (EDS), and that a reliable quantification of oxygen was not possible, we adopt the designation $Ti_4Fe_2O_x$, except for the HEXRD evaluation where the composition $Ti_4Fe_2O_{0.4}$ was used. According to Zemek et al. [14] the oxygen content of this phase can vary between 4 and 14.3 at.%, corresponding to $Ti_4Fe_2O_x$ with $0.25 < x < 1$. This phase is usually referred to as η in the literature [12].

## A6. Determination of phase density from NF-PXCT

In spite of adequate segmentation of the phases (see manuscript, Fig. 3), the grey value gradient at the interface between the phases obtained in NF-PXCT reconstructions, especially in the ultrafine eutectic regions of TiFe and β-Ti, affects the estimation of the mass density. This grey value gradient is a consequence of the spatial resolution limitation (see supplementary material, Fig. S1) that tends to blur the interface between phases. A more suitable approach is rather to select a sufficiently large region within a phase (far enough from the interface to a second phase) to calculate the local mass density. Taking this into account, the mass density histograms were calculated considering regions such as the colour-coded ones shown in Fig. S4a

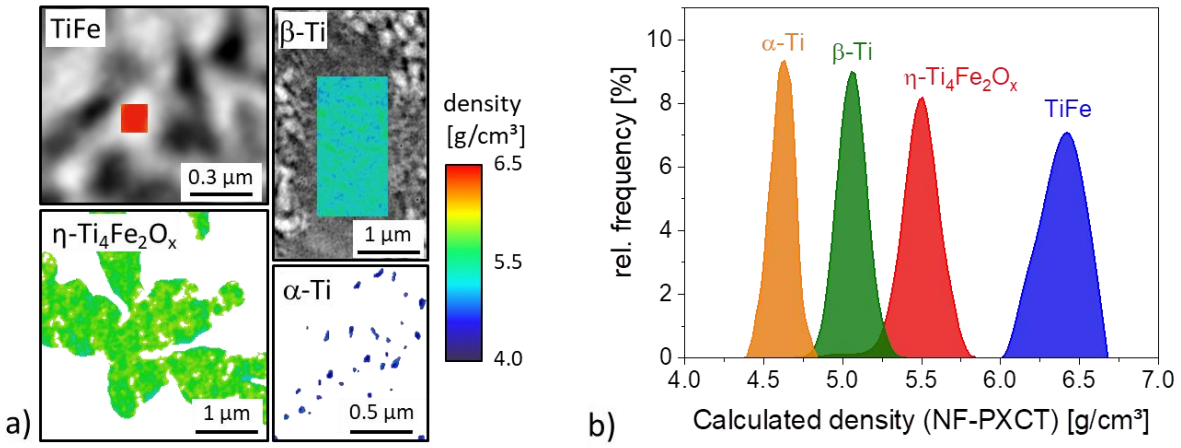


**Fig. S4: Representative colour-coded 2D NF-PXCT slices of LPBF-Ti-32Fe considered for the quantification of local mass density. The selected regions for TiFe and β-Ti are enclosed by a box located far enough from the border of the phase (a). Mass density histograms for selected areas of the different phases (b).**

## References:


[1] J.-C. Labiche et al., Rev. Sci. Instrum. 78 (9) (2007) 091301
[2] M. Stockmar et al., Sci. Rep. 3 (1) (2013) 1927
[3] A. Kaestner et al., Opt. Eng. 50 (12) (2011) 123201
[4] B. Enders, P. Thibault, Proc. R. Soc. A 472 (2196) (2016) 20160640
[5] P. Thibault et al., Science 321 (5887) (2008) 379

[6] P. Thibault, M. Guizar-Sicairos, New J. Phys. 14 (6) (2012) 063004
[7] M. Guizar-Sicairos et al., Opt. Express 19 (22) (2011) 21345
[8] J. C. da Silva et al., High energy near- and far-field ptychographic tomography at the ESRF. In *SPIE Optical Engineering + Applications*, SPIE(2017), Vol. 10391
[9] M. van Heel, M. Schatz, J. Struct. Biol. 151 (3) (2005) 250
[10] T. Hildebrand, P. Rüegsegger, J. Microsc. 185 (1) (1997) 67
[11] R. Ray et al., Metall. Mater. Trans. B 3 (3) (1972) 627
[12] B. Rupp, P. Fischer, J. Less-Common Met. 144 (2) (1988) 275
[13] M. K. Thomas, R. E. Trabocco, Unidirectionall solidified titanium base eutectics with iron, conbalt, nickel. In *Proceedings of the Conference on In Situ Composites*, NMAB National materials Advisory Board, Lakeville Connecticut, (1972), Vol. 1
[14] O. Zemek et al., Monatshefte für Chemie 100 (1969) 2075
[15] O. Heinen, Nahordnung und Erstarrung unterkühlter Schmelzen von Ti-Basis Legierungen. Dissertation, Ruhr-Universität Bochum, 2005
[16] W. Rostocker, J. Met. January (1955) 113